Proceedings of the ASME 2016 Fluids Engineering Division Summer Meeting
FEDSM2016
July 10-14, 2016, Washington, DC, USA

FEDSM2016-7895

MODELING SEPARATION AND CAVITATION BEHIND A BLUNT BODY

Jingsen Ma
DYNAFLOW, INC.
www.dynaflow-inc.com
10621-J Iron Bridge Road, Jessup, MD, USA
jingsen@dynaflow-inc.com

Chao-Tsung Hsiao
DYNAFLOW, INC.
www.dynaflow-inc.com
10621-J Iron Bridge Road, Jessup, MD, USA
ctsung@dynaflow-inc.com

Xiongjun Wu
DYNAFLOW, INC.
www.dynaflow-inc.com
10621-J Iron Bridge Road, Jessup, MD, USA
wxj@dynaflow-inc.com

Georges L. Chahine
DYNAFLOW, INC.
www.dynaflow-inc.com
10621-J Iron Bridge Road, Jessup, MD, USA
glchahine@dynaflow-inc.com

ABSTRACT

Cavitation flow behind a blunt body is modeled using a physics-based numerical model of cavitation initiation and transition to larger cavities. The calculations initiate from the dynamics of nuclei, then tracks the dispersed bubble phase with a two-phase viscous model. This solver includes a level set method to model coalescence of the nuclei into large cavities and to track the dynamics of the resulting free surfaces. A transition scheme enables collection of the bubbles into a large cavity and also enables breakup of a large cavity into a bubble cloud.

Using this model, simulations are conducted for different flow velocities and corresponding cavitation regimes. When the velocity is relatively small (i.e., large cavitation number), flow separation behind the body results in the shedding of vortices, which capture nuclei in their cores to form elongated vortical cavities. As the flow velocity increases (or as the ambient pressure decreases) the flow evolves into a separated flow with a large cavity behind the body. A reentrant jet may form and move upstream into the cavity towards the body. This jet periodically shears off portions of the cavity volume, resulting in large amounts of bubble clouds. These results are in good qualitative agreements with experimental observations.

INTRODUCTION

Bubbly flow problems have a wide spectrum of applications in marine hydrodynamics [e.g.,1-6]. Numerical modeling of this kind of problems, especially while involving cavitation, remains challenging due to its complex physics. Cavitation on a body depends on the cavitation number, σ,

$$\sigma = \frac{P_\infty - P_v}{0.5\rho V^2}, \tag{1}$$

where P_∞ is the free stream static pressure, P_v is the vapor pressure, V is the characteristic flow velocity, and ρ is the liquid density. As σ becomes very low the flow enters the supercavitation regime where the length of the large cavity becomes greater than the body length [6-9]. In order to achieve a small σ, either a high free stream velocity or a small pressure difference P_∞ - P_v is needed. Underwater moving bodies can encounter several regimes of cavitation as the speed increases, including partial cavitation and supercavitation.

To model all stages a multiscale approach is needed since a large range of length and time scales are involved; e.g. a large scale for the super cavity dynamics, a much smaller scale for the micro bubbles, and an intermediary scale for the bubble clouds [10,11]. As a result, accurate prediction of various cavitation regimes behind a submerged body requires a two-phase flow model which can address the incipient mechanism as well as the multiple length scale nature of the problem.

To this end we have developed a multiscale method, which integrates a Lagrangian Discrete Singularity Model (DSM) for dispersed nuclei and bubbles with an Eulerian viscous description of the two-phase medium [12-16]. A level set method is included in the Eulerian code to model free surfaces and large cavities, along with a transition scheme to smoothly

transform growing or collecting bubbles into large cavities and breakup large cavities into bubble clouds. This method has been successfully applied for sheet cavitation on hydrofoils [12-16]. In this paper, this method is extended to simulate the various cavitation stages behind a moving blunt body under various speeds, which we had previously experimentally studied in a controlled laboratory setting [6].

NUMERICAL METHODOLOGY

The 3D multiscale model, including the inter-scale transition schemes, employed in this study has been extensively validated and documented in our previous studies of sheet cavitation [12,14,16], gas core formation in space separators [13] and propeller flow [15], … etc. The present paper addresses its applications extended into the multi-stage cavitation over moving bodies and do not consider additional model development. Therefore, below we only provide a brief summary of the key features of the model to avoid unnecessary repeats. Readers interested in more details on modeling aspects may refer to the references provided above.

Eulerian Continuum Model for Carrier Fluid Phase

The unsteady Navier-Stokes equations can be written as follows:

$$\frac{\partial \rho_m}{\partial t} + \nabla \cdot \left(\rho_m \mathbf{u} \right) = 0, \tag{2}$$

$$\rho_m \frac{D\mathbf{u}}{Dt} = -\nabla p + \mu_m \nabla^2 \mathbf{u} + \rho_m \mathbf{g}, \tag{3}$$

where $\mathbf{u}$ is the mixture velocity, p the pressure and $\mathbf{g}$ the acceleration due to gravity. The mixture density ρ_m and the mixture viscosity, μ_m, are related to the void fraction, α, and the liquid and gas properties through

$$\begin{aligned} \rho_m &= (1-\alpha)\rho_l + \alpha\rho_g, \\ \mu_m &= (1-\alpha)\mu_l + \alpha\mu_g. \end{aligned} \tag{4}$$

α is obtained from the space distribution and size information of the bubbles. The influence of each bubble is spread using a Gaussian distribution conserving the total bubble volumes [17].

Equations (2) and (3) are solved using the Eulerian flow solver 3DYNAFS-VIS© [18]. The numerical scheme uses a finite volume formulation. A first-order Euler implicit difference formula is applied to the time derivatives. The spatial differencing of the convective terms uses the flux-difference splitting scheme based on a van Leer's MUSCL method [19] for obtaining the third-order fluxes. A second-order central differencing is used for the viscous terms.

Level-Set Method for Large Bubbles and Cavities

A level-set method [20-22] is adopted to handle large bubbles and cavities because the level-set method offers a flexible way to resolve large free surface deformations such as folding and breakup as compared to a surface tracking methods which require to actually discretize the interfaces. A smooth distance function, φ (x,y,z,t), whose zero value coincides with the liquid/gas interface, is defined in the computational domain as the signed distance from the interface. This function is enforced to be a material surface at each time step using:

$$\frac{\partial \varphi}{\partial t} + u_j \frac{\partial \varphi}{\partial x_j} = 0. \tag{5}$$

To avoid that the value of φ gets diffused by numerical errors and become distorted by the flow field, a re-initialization distance function is constructed by solving a "re-initialization equation" in pseudo time iterations [22].

In a standard level-set approach both liquid and gas phases of the fluid are solved separately using Equations (2) and (3) after identifying to which phase the cell belongs and applying appropriate interfacial boundary conditions. However, we found a simpler single phase level-set method more appealing. This single phase level-set approach consists of using the Ghost Fluid Method [22] to impose the dynamic boundary conditions across the interface without applying any smoothing function. The dynamics boundary condition requires continuity of stresses across the surface. This is satisfied by assuming balance of normal stresses and zero shears, as usually done in single-phase Level Set methods [20-22].

Discrete Singularity Model (DSM) for Bubbles

All bubbles are treated as point sources to account for volume change and dipoles to account for translation. The equivalent spherical bubble radius, R(t), is obtained using a modified Rayleigh-Plesset-Keller-Herring equation [23] which accounts for the surrounding medium compressibility and for non-uniform pressure field [24,25]. This is achieved by adding an pressure term due to bubble slip velocity and using Surface Averaged quantities on the bubble [23-25]:

$$\begin{aligned} \left(1-\frac{\dot{R}}{c}\right) R\ddot{R} + \frac{3}{2}\left(1-\frac{\dot{R}}{3c}\right)\dot{R}^2 &= \frac{\left(\mathbf{u}_{enc} - \mathbf{u}_b\right)^2}{4} \\ &+ \frac{1}{\rho}\left(1+\frac{\dot{R}}{c}+\frac{R}{c}\frac{d}{dt}\right)\left[p_v + p_g - p_{enc} - \frac{2\gamma}{R} - 4\rho\nu\frac{\dot{R}}{R} \right]. \end{aligned} \tag{6}$$

c and ρ are the sound speed and density of the fluid, respectively. p_v is the liquid vapor pressure, and γ is the surface tension. $\mathbf{u}_b$ is the bubble center velocity and p_{enc} and $\mathbf{u}_{enc}$ are the fluid pressures and velocities averaged over the bubble surface. Specifically, these quantities are obtained through an arithmetic averaging of the mixture pressures and velocities at six polar points on the bubble surface. The mixture quantities are interpolated from the mixture flow solutions in the neighboring fluid cells. This averaging procedure is to account for non-uniform pressures and velocities along the bubble surface [24,25]. The introduction in Equation (6) of

$(\mathbf{u}_{enc}- \mathbf{u}_b)^2/4$ is to account for slip between the bubble and the host medium. The bubble trajectory is obtained using the following equation of motion [26]:

$$\frac{d\mathbf{u}_b}{dt} = -\frac{3}{\rho}\nabla p - 2g + \frac{3}{4}\frac{C_D}{R}\left(\mathbf{u}_{enc} - \mathbf{u}_b\right)\left|\mathbf{u}_{enc} - \mathbf{u}_b\right| + \frac{3}{2\pi}\frac{C_L}{R}\sqrt{\nu}\frac{(\mathbf{u}_{enc} - \mathbf{u}_b)\times\boldsymbol{\omega}}{\sqrt{|\boldsymbol{\omega}|}} + \frac{3}{R}(\mathbf{u}_{enc} - \mathbf{u}_b)\dot{R}, \quad (7)$$

where C_L is the lift coefficient [27], $\boldsymbol{\omega}$ is the local vorticity, and C_D is a drag coefficient [28]:

$$C_D = \frac{24}{R_{eb}}\left(1 + 0.197 R_{eb}^{0.63} + 2.6\times10^{-4} R_{eb}^{1.38}\right), \qquad R_{eb} = \frac{2\rho R\left|\mathbf{u}_{enc} - \mathbf{u}_b\right|}{\mu}. \quad (8)$$

Transition Scheme

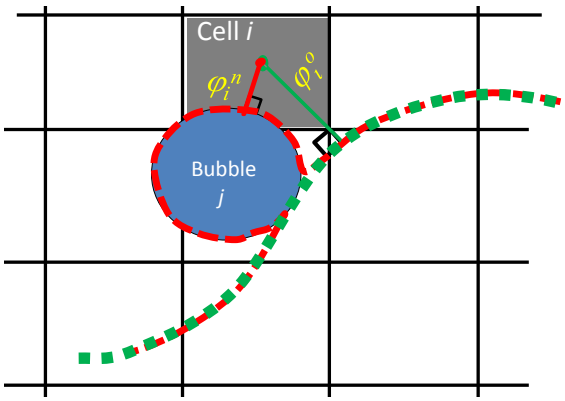

Figure 1: Illustration of a bubble merging into a pre-existing free surface. Green dash curve is the old free-surface and the red dash curve is the new surface after the merger. φ_i^o and φ_i^n are the distance function values of a cell *i* before and after the merger.

A transition scheme [12-16] was implemented to transform a bubble, which grows more than a given limit, from a singularity into a large cavity or gas/liquid interface represented by level set zero. The criterion is based on the bubble size and/or on the local void fraction and the subject bubble *j*, is activated for computation of a local distance function for all neighboring cells. For each cell *i*, the distance function is then defined by:

$$\varphi_i = \min(\varphi_{LS0}, \varphi_{b,j}) \quad j = 1, N_i \quad (9)$$

where φ_{LS0} is the original distance function from the level set computation, $\varphi_{b,j}$ is the local distance function computed based on the surface of bubble, *j* and N_i is the number of bubbles which are "activated" around cell *i*. Note this scheme not only allows multiple bubbles to merge together into a large cavity, but also enables a single bubble to merge with a pre-existing large cavity as illustrated in Figure 1 .

PROBLEM DESCRIPTION AND SIMULATION SETUP

Using the above described multiscale model, we simulated the separation and cavitation flow behind a submerged blunt body at different velocities. Figure 2 shows snapshots of the cavitating flow behind the body at different speeds from our experimental study [6]. Since the previous study only focused on the content of cavity, the experimental observations in the study can now only provide qualitative comparisons.

Figure 3 (top) shows the layout and dimensions of the test section where the experiments were conducted. It consists of 3 segments which have different expansion profiles. The short flow entrance section with a length of 2 in, where the bullet is mounted, has a constant cross section and is where the cavity. The test section then gradually expands to to maintain near constant pressure over the cavity. At the end of the test section, a high expansion 1 ft portion keeps the flow from separating behind the cavity. The flow there slows down and the local pressure increases to reach the atmospheric pressure at the exit. The two parallel side walls of the acrylic test section were 1 in. apart, which is significantly, smaller than the section length allowing a simplification as a 2D problem. An 11-block mesh with ~20,000 grid points was created for the simulation (Figure 3 bottom). The mesh was made finer in the region of interests, i.e., close to the body, and gradually became coarse downstream and upward of it.

A very important aspect of our approach is to account for nucleation from the rigid boundaries [14,16] in addition to bubble nuclei dispersed in the liquid. The wall nucleation model involves the following parameters, which are functions of the wall material properties and the local flow conditions:

a) P_{thr}, a nucleation pressure threshold,

b) N_s, a number density of nucleation sites per unit area,

c) f_n , a nucleation rate, and

d) R_0, initial nuclei size(s).

At each time step the pressure at a cell is compared with P_{thr} to determine if nucleation should occur. Once the pressure is lower than the threshold, the cell releases a *N* nuclei in Δt, the time interval between two flow solver time steps. *N* is given by:

$$N = N_s f_n \Delta t \Delta A, \quad (10)$$

where ΔA is the surface area of the local cell. Since bubble computations require much smaller time steps than the Eulerian flow solver, the *N* nuclei can be released randomly in time and in space during the time step. In the results below, P_{thr} is selected to be the vapor pressure. The initial size of the nuclei emitted is selected to be 10 μm with the base nucleation sites per unit area value selected to be N_s = 224/cm^2 and the base nucleation frequency selected to be f_n = 22*kHz*. These

parameters are selected based on [14], where the results became independent of N_s and f_n when larger than these values.

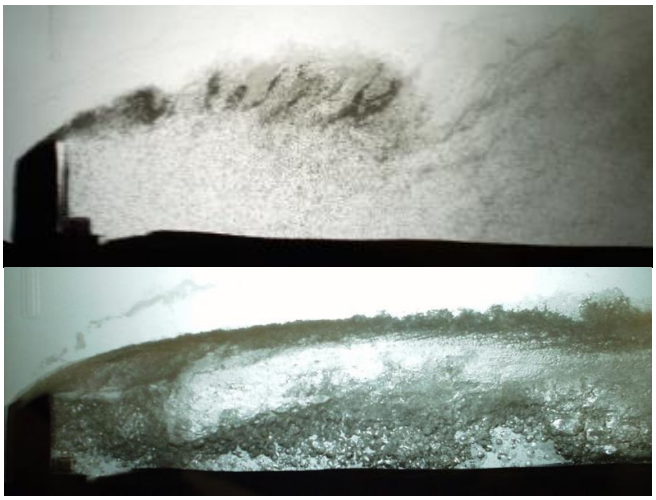

Figure 2. Pictures of the cavitating flow behind a blunt body at low (top) and high (bottom) speeds [6].

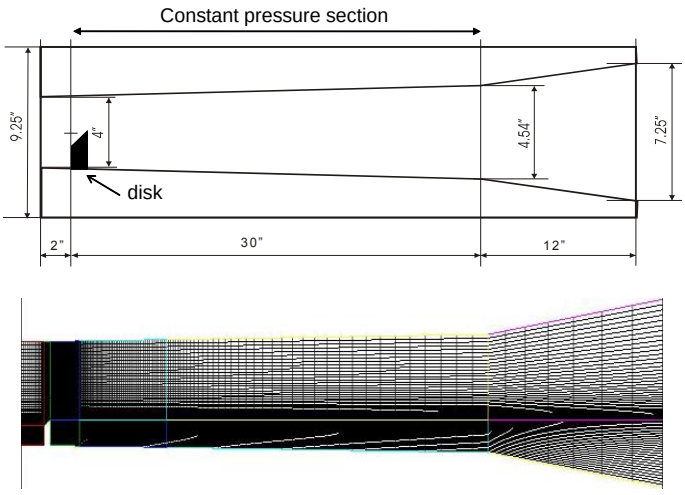

Figure 3. Setup of separated flow experiments and simulation. A) Sketch of the test section with dimension (stretched along the vertical direction) B) The 2D mesh generated for simulation.

SIMULATION RESULTS & DISCUSSION

Vortical Structures and Cavitation Inception

Flow separation behind the blunt body results in the shedding of vortices, which capture nuclei at their centers, causing them to grow and collect in the low-pressure vortical regions. With the local pressure decreases below the vapor pressure, cavitation inception occurs in these vortices. This is clearly seen in Figure 2 –top and in Figure 4. In the top picture in Figure 4 the flow field is shown with vorticity contours in order to highlight the large vortical structures formed behind the body. The cores of these vortical structures are low pressure regions which could lead to explosive nuclei growth and cavitation. This is evidenced by the bottom picture in the same figure, where it is seen that the pressure in some core centers drops below 2300 Pa, the water vapor pressure. Bubble clusters are also observed in these cores, which merge and become elongated cavities. The former are simulated by DSM bubbles while the latter are described by free surface dynamics using the level set method.

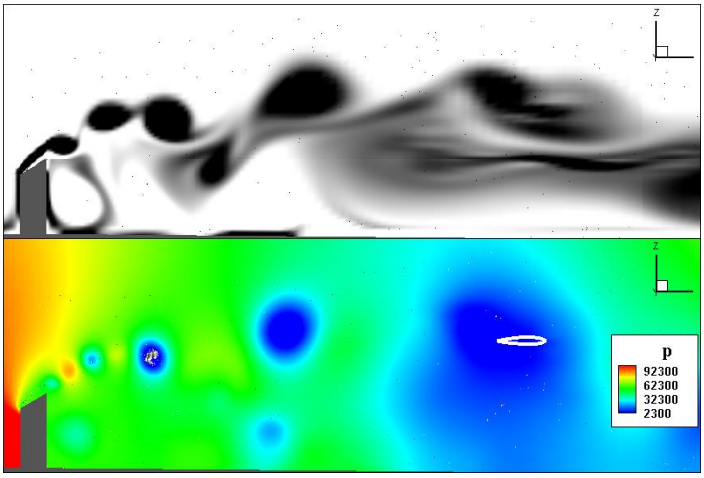

Figure 4. Top: Large vortical structures formed behind the body; Bottom: Entrainment of nuclei bubbles into the low-pressure vortical centers and cavitation inception . The color contours represent the pressure, while the silver spheres are the nuclei bubbles and the white lines correspond to the zero level set cavity interface.

A time sequence of the two-phase flow development behind the body is shown in Figure 5. This highlights nuclei capture and cavitation inception by the multiscale method. In particular, sequences (a) and (b) indicate that the inception can be modeled by enabling the collected bubbles to form an initial cavity. This is achieved with the help of the level set method in the continuum two-phase viscous model. As the bubbles grow beyond a threshold size and/or as bubbles merge, the model initiates a gas-liquid interface dynamics described by the level set method. The initiated cavity continues its growth while elongating. It then starts to shrink as it travels further downstream, since the pressure increases as the vorticity becomes weaker while moving downstream (see Figure 5 c).

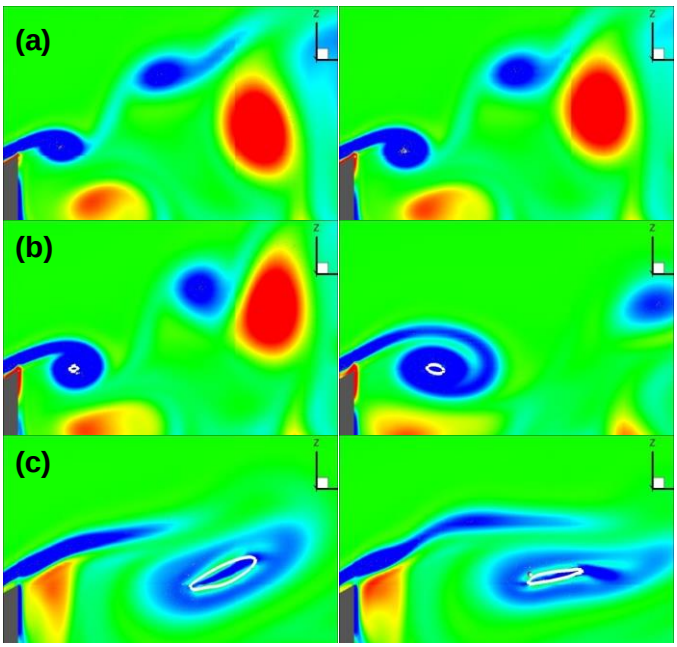

Figure 5. A time sequence of the flow behind the body, showing: (a) bubble entrainment, (b) cavitation inception and (c) cavity deformation and shrinkage due to the vortical structure evolution behind the body for the 6 m/s case. Color contours represent vorticity. Silver spheres are the nuclei bubbles and the white line corresponds to the zero level set cavity interface.

Cavitation under Different Flow Velocities

The pressure on the body edges decreases as the flow rate increases. The evolution of the cavitating flow from cavitation inception, to limited cavitation and supercavitation is shown in Figure 6. Figure 6a shows at a relatively low flow rate, the shedding vortices carrying downstream bubbles generated from cavitation on the body. With increased flow rate, as shown in Figure 6b, the bubbles generated from the intensified cavitation become denser and the cavities become larger. This trend continues with further increase in the flow rate and partially overlapping cavities start occupying large regions (Figure 6 c). At the end a supercavity is formed as seen in Figure 6d and Figure 6 e. The supercavity is not stable and an unsteady reentrant jet enters periodically the cavity against the main flow direction as shown in Figure 6e. This appears as a turbulent mass of liquid moving upstream in the cavity toward the projectile. The impact of this reentrant jet on the projectile is strong enough to completely break the supercavity off the body as seen in Figure 7 which illustrates a sequence of reentrant jet underneath the supercavitation moving towards the body.

SUMMARY AND FUTURE WORK

Modeling the various cavitation stages behind a blunt body was accomplished using a multiscale two-phase flow Eulerian-Lagrangian model. The two-phase medium was modeled as a continuum flow, while a Discrete Singularity Model was used for the dispersed phase. A level set method was used to describe free surfaces and macro cavities, along with a transition scheme to smoothly transform growing or collecting microbubbles into large cavities.

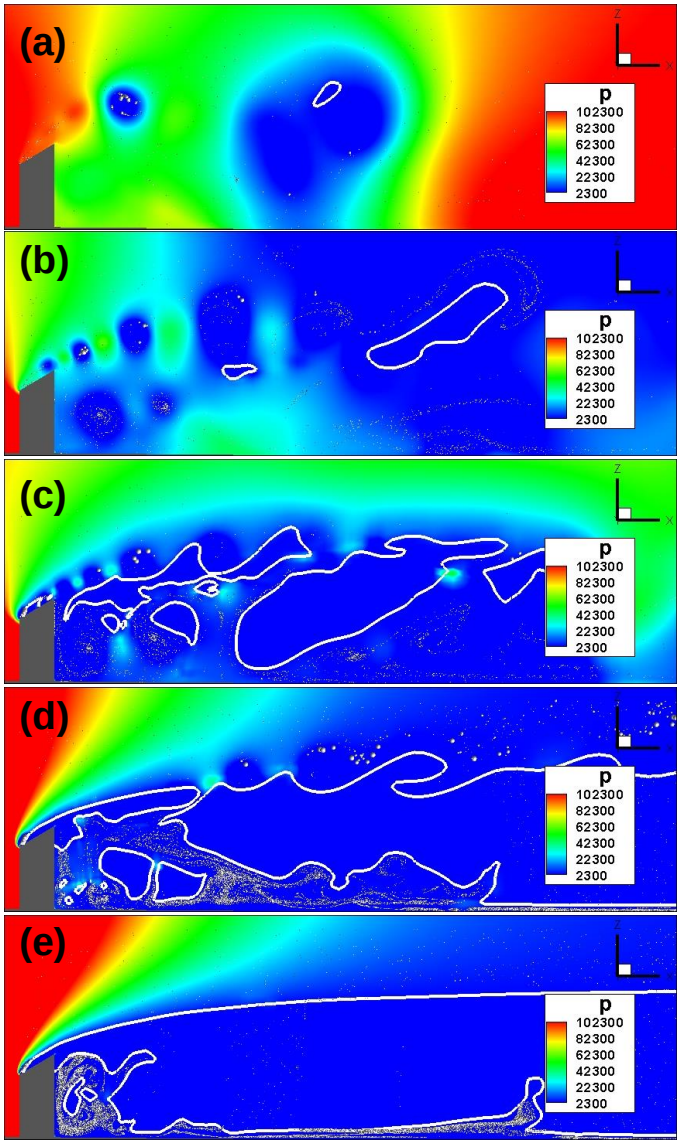

Figure 6. Evolution of the cavitating flow from cavitation inception and limited cavitation to supercavitation under increasingincoming speeds: (a) 6 m/s; (b) 8 m/s; (c) 12 m/s; (d) 15 m/s and (e) 18 m/s. Color contours represent vorticity. Silver spheres are the nuclei bubbles and the while line correspond to the zero level set cavity interface.

All stages of the cavitating flow including cavitation inception, separated flow wake cavitation, and supercavitation were directly captured by the method simply through tracking the dynamics of bubble nuclei in the flow. When the body velocity is relatively small, flow separation behind the body results in the shedding of vortices, which capture nuclei in their cores and transforms them into elongated vortical cavities. As

the body velocity increases or as the ambient pressure decreases, the flow evolves into a separated cavitating flow, then into a large supercavity filled of gas and vapor. A reentrant jet forms periodically and moves upstream into the cavity towards the body. These results are in good qualitative agreements with experimental observation previously conducted in a controlled laboratory setting.

ACKNOWLEDGEMENTS

This work was supported by the Department of Energy under an SBIR Phase II contract DE-FG02-07ER84839. The authors would also like to acknowledge support from the Office of Naval Research under contract N00014-12-C-0382 monitored by Dr. Ki-Han Kim.

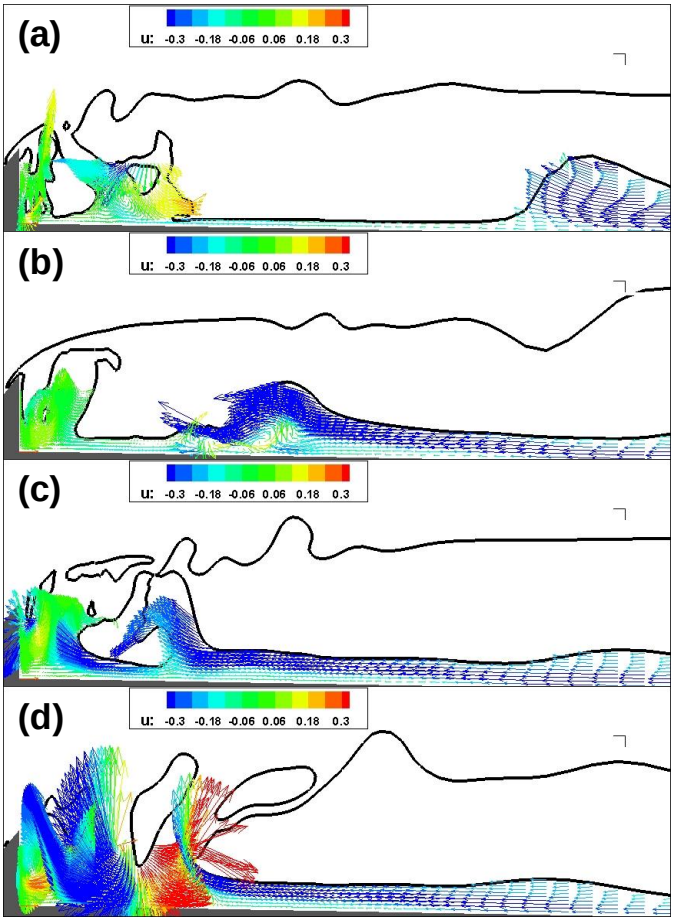

Figure 7. A time sequence of reentrant jet underneath the supercavitation. (The color arrows represent velocity vectors, and the black line corresponds to the cavity interface represented by iso-surface of zero level set).

REFERENCES

1. Ma, J., Oberai, Drew, D.A., Lahey, R.T., Jr,, and Moraga, F., 2010, "A quantitative sub-grid air entrainment model for bubbly flows-plunging jets" *Computers & Fluids*, 39: pp. 77-86.
2. Ma, J., Oberai, A., Hyman, M., Drew, D.A., and Lahey, R.T., Jr, 2011, "Two-Fluid Modeling of Bubbly Flows around Surface Ships Using a Phenomenological Subgrid Air Entrainment Model." *Computers & Fluids*, 52, pp. 50-57.
3. Ma, J., Oberai, A., Drew, D.A., and Lahey, R.T., Jr, 2012, "A Two-Way Coupled Polydispersed Two-Fluid Model for the Simulation of Air Entrainment beneath a Plunging Liquid Jet." *ASME Journal of Fluids Engineering*, 134(10), pp.101304
4. Xiang, M., Cheung, S., Yeoh, G., Zhang, W., and Tu, J., 2011, "On the numerical study of bubbly flow created by ventilated cavity in vertical pipe.", *Int J Multiphase Flow*, 2011, 37(7), pp.756–768
5. Hsiao, C. T., Wu, X., Ma, J. and Chahine, G. L. 2013. "Numerical and experimental study of bubble entrainment due to a horizontal plunging jet". *International Shipbuilding Progress*, 60, pp. 435-469.
6. Wu, X. and Chahine, G., 2007 "Characterization of the Content of the Cavity Behind a High-Speed Supercavitating Body", *ASME Journal of Fluids Engineering*, 129, pp. 136-145
7. Stinebring, D., Billet, M., Lindau, J. and Kunz, R., 2001, "Developed cavitation – cavity dynamics," VKI Lecture Series.
8. Wosnik, M., Schauer, T, and Arndt, R., 2003, "Experiment study of a ventilated supercavitating vehicle", CAV2003, Proceedings of the Fifth International Symposium on Cavitation, Osaka, Japan.
9. Kirschner, I., Moeny, M., Krane, M. and Kinzel, M., 2015, "Jet-Supercavity Interaction: Insights from Physics Analysis", *Journal of Physics: Conference Series*, 656 (1), pp. 01215.1-4.
10. Ma, J, Hsiao, C-T. and Chahine, G.L., 2015, "Euler–Lagrange Simulations of Bubble Cloud Dynamics Near a Wall", ASME Journal of Fluid Engineering, 137(4), pp.041301.
11. Ma, J, Hsiao, C-T. and Chahine, G.L., 2015, "Shared-Memory Parallelization for Two-Way Coupled Euler–Lagrange Modeling of Cavitating Bubbly Flows", ASME Journal of Fluid Engineering, 137(12), pp.121106.
12. Ma, J, Hsiao, C-T. and Chahine, G.L., 2013, "Multiscale Modeling of Cavitating Bubbly Flows", *Bulletin of the American Physical Society*, 58.
13. Ma, J., Hsiao, C.-T., and Chahine, G.L. 2014 "Numerical Modeling of Bubbly Two-Phase Flow in a Vortex Separator". *9th Int'l Conference on Two-Phase Systems for Ground and Space Applications*, Baltimore, MD, September 22-26.
14. Hsiao, C.-T., Ma, J., and Chahine, G.L. 2014, "Multi-Scale Two-Phase Flow Modeling of Sheet and Cloud Cavitation". *30th Symposium on Naval Hydrodynamics*, Hobart, Tasmania, Australia, November 2-7,.
15. Hsiao, C.-T., Ma, J., and Chahine, G.L. 2015, "Simulation

of Sheet and Tip Vortex Cavitation on a Rotating Propeller Using a Multiscale Two-Phase Flow Model". *Fourth International Symposium on Marine Propulsors*, Austin, Texas, USA, June 1-4, 2015
16. Ma, J., Hsiao, C-T., and Chahine, G.L. 2015 "Modelling Cavitating Flows using an Eulerian-Lagrangian Approach and a Nucleation Model". *Journal of Physics: Conference Series*, 656 (1), pp. 12160.1-4.
17. Ma, J., Chahine, G.L., and Hsiao, C-T. "Spherical Bubble Dynamics in a Bubbly Medium using an Euler–Lagrange Model". *Chemical Engineering Science*, Vol. 128, pp. 64–81, May 2015.
18. Chorin, A. J., 1967, "A Numerical Method for Solving Incompressible Viscous Flow Problems," Journal of Computational Physics, 2, pp. 12-26.
19. Van Leer, B., Thomas, J.L., Roe, P.L. and Newsome, R.W., 1987, "A Comparison of Numerical Flux Formulas for the Euler and Navier-Stokes Equation," AIAA Paper No. 87-1104-CP.
20. Sussman, M., P. Smereka, and S. Osher, A level set approach for computing solutions to incompressible two-phase flow. *Journal of Computational Physics*, 1994. 114(1): p. 146-159.
21. Osher, S. and R.P. Fedkiw, Level set methods: an overview and some recent results. *Journal of Computational Physics*, 2001. 169(2): p. 463-502.
22. Sussman, M., et al., An improved level set method for incompressible two-phase flows. Computers & Fluids, 1998. 27(5): p. 663-680.
23. Plesset, M.S. and Prosperetti, A., 1977, "Bubble Dynamics and Cavitation," Annual Review of Fluid Mechanics, 9, pp.145-185.
24. Chahine, G. L., 2009, "Numerical Simulation of Bubble Flow Interactions", Journal of Hydrodynamics, Vol. 21 (3), pp 316-332.
25. Hsiao, C.-T., Chahine, G. L. and Liu, H.-L. , 2003, "Scaling Effects on Prediction of Cavitation Inception in a Line Vortex Flow", ASME Journal of Fluid Engineering, 125, pp.53-60.
26. Johnson, V.E. and Hsieh, T. , 1966, "The Influence of the Trajectories of Gas Nuclei on Cavitation Inception," Sixth Symposium on Naval Hydrodynamics, pp. 163-179.
27. Saffman, P., The lift on a small sphere in a slow shear flow. Journal of Fluid Mechanics, 1965. 22(02): p. 385-400.
28. Haberman, W.L. and Morton, R.K., 1953, "An Experimental Investigation of the Drag and Shape of Air Bubbles Rising in Various Liquids," Report 802, DTMB.